The Orbital Distribution of Satellite Galaxies

Stéphane Herbert-Fort¹, Dennis Zaritsky¹, Yeun Jin Kim^{2,1}, Jeremy Bailin^{3,4}, and James E. Taylor⁵

- ¹ University of Arizona/Steward Observatory, 933 N Cherry Avenue, Tucson, AZ 85721 (email: shf@as.arizona.edu)
- ²Department of Astronomy and Astrophysics, University of Chicago, 5640 S. Ellis Avenue, Chicago, IL 60637
- ³ Department of Physics & Astronomy, ABB-241, McMaster University, Hamilton, ON, L8S4M1, Canada
- ⁴Centre for Astrophysics & Supercomputing, Swinburne University, Hawthorn, VIC 3122, Australia
- ⁵ Department of Physics & Astronomy, University of Waterloo, Waterloo, ON, N2L3G1, Canada

Accepted 2007 November 21

ABSTRACT

We measure the distribution of velocities for prograde and retrograde satellite galaxies using a combination of published data and new observations for 78 satellites of 63 extremely isolated disc galaxies (169 satellites total). We find that the velocity distribution is non-Gaussian (> 99.9% confidence), but that it can be described as the sum of two Gaussians, one of which is broad ($\sigma = 176 \pm 15 \text{ km s}^{-1}$), has a mean prograde velocity of $86 \pm 30 \text{ km s}^{-1}$, and contains $\sim 55\%$ of the satellites, while the other is slightly retrograde with a mean velocity of -21 ± 22 km s⁻¹ and $\sigma = 74 \pm 18$ km s⁻¹ and contains $\sim 45\%$ of the satellites. Both of these components are present over all projected radii and found in the sample regardless of cuts on primary inclination or satellite disc angle. The double-Gaussian shape, however, becomes more pronounced among satellites of more luminous primaries. We remove the potential dependence of satellite velocity on primary luminosity using the Tully-Fisher relation and still find the velocity distribution to be asymmetric and even more significantly non-Gaussian. The asymmetric velocity distribution demonstrates a connection between the inner, visible disc galaxy and the kinematics of the outer, dark halo. The reach of this connection, extending even beyond the virial radii, suggests that it is imprinted by the satellite infall pattern and large-scale effects, rather than by higher-level dynamical processes in the formation of the central galaxy or late-term evolution of the satellites.

Key words: galaxies: evolution – galaxies: haloes – galaxies: structure – dark matter

1 INTRODUCTION

Although it is now generally accepted that galaxies are embedded in large (>100 kpc), massive (> $10^{12}M_{\odot}$) dark matter haloes, the detailed spatial and kinematic structure of those haloes, and the relationships between that structure and the resulting optical galaxy, remain largely unknown. The particulars of the process of accretion and assembly are usually deduced from simulations because the inner galaxy, which is what we can easily observe, has been scrambled by its complex physical evolution. We seek empirical evidence, in the outer dark halo, of how disc galaxies grow and signatures of a connection between the outer halo and the inner galaxy. The only tracers that are sufficiently luminous and distant from the central galaxy are satellite galaxies (Zaritsky et al. 1993; Zaritsky et al. 1997, hereafter ZSFW).

Two relatively recent advances justify a re-examination of this topic. First, the sample of spectroscopically confirmed satellites has grown by more than an order of magnitude

recently due to the Two-Degree Field Galaxy Redshift Survey (2dFGRS; Sales & Lambas 2004, 2005) and the Sloan Digital Sky Survey (SDSS; Prada et al. 2003). Second, a slew of new simulations is aimed at explaining/predicting the properties of satellite galaxies (e.g. Knebe et al. 2004; van den Bosch et al. 2005; Zentner et al. 2005; Azzaro et al. 2006; Sharma & Steinmetz Libeskind et al. 2007; Sales et al. 2007). Overall, simulations agree that infalling material is critical to the formation of galaxies and that satellites should bear some imprint of this infall. Some naive scenarios suggest potential signatures. First, for a homogeneous collapse model of galaxy formation (in which the satellites are unbiased fragmented debris of the process; e.g. Maller & Bullock 2004), one would predict a high degree of alignment between the disc and satellite angular momenta because both arise from the same parent population. In contrast, in a hierarchical model, one might expect late-coming satellites, those preferentially found at large radii, to have little connection to the central disc. To complicate matters further, in a model with strong dynamical evolution one would expect slow prograde satellites, which experience the largest dynamical friction, to be underrepresented. In actuality, all of these effects (and others) compete, and so detailed numerical simulations in a cosmological framework are necessary to make quantitative predictions.

Simulations attempting the necessary level of detail are overwhelmingly expensive because of the required resolution over cosmological volumes. This difficulty becomes particularly acute when one realizes that defining the observational sample requires careful selection from large redshift catalogues (see Bailin et al. 2007, hereafter B07) to ensure that one has found the dynamically isolated systems, and hence that similar volumes must be simulated to identify a truly corresponding sample in simulations. It is insufficient simply to identify random disc galaxies in simulations because the criteria for defining the observational sample is far more restrictive. Until recently (Okamoto et al. 2005; Governato et al. 2007; Libeskind et al. 2007, hereafter L07), ACDM galaxy formation simulations had been unable to create satellite populations of resolved and realistic spiral galaxies with properties similar to those of the Local Group. Because the simulations are currently unable to provide reliable guidance on dynamical signatures of galaxy assembly and formation that might be present in the most isolated systems residing in large-scale cosmological volumes, we search for any signatures in observational samples.

One such signature that has received significant attention is the angular anisotropy in the distribution of satellites around isolated disc galaxies (e.g. Holmberg 1969; Zaritsky et al. 1997b; Sales & Lambas 2004; Brainerd et al. 2005), often referred to as the Holmberg effect, even though the results regard the satellite distribution over a significantly different, and possibly physically distinct, range of projected radii than that explored in the original study. This anisotropy, if confirmed, likely has its roots in the anisotropic infall of satellites along filaments (e.g. Aubert et al. 2004; Knebe et al. 2004), but simulations have so far failed to fully explain it primarily because they have difficulties in realistically forming the central galaxies and satellite populations in a cosmological context. The possible detection of satellite anisotropy to large radii (out to $\sim 500~h_{75}^{-1}$ kpc; Zaritsky et al. 1997b), dynamical studies (Prada et al. 2006), and weak lensing studies (Guzik & Seliak 2002) all suggest that the haloes of these galaxies are quite extended, that there is a connection between the central galaxy and the outer halo that extends even beyond the virial radius, and that these satellites may provide additional clues linking the inner and outer galaxy.

Our goal is modest: we search for additional such signatures connecting the inner, observable, disc galaxy and the outer, dark halo by exploring the distribution of satellite angular velocities relative to the disc. Most studies of satellite dynamics only measure the difference in recessional velocities, Δv_{rec} , between primary and satellite. ZSFW, in addition, measured the rotation sense of the primary and were therefore able to measure, in projected space, whether a satellite was on a prograde or retrograde orbit. With their limited sample size, they focused on measuring the prograde fraction, which they found to be slightly above

0.5. Since ZSFW, both the angular anisotropy and rotation results have been revisited, with conflicting results (Sales & Lambas 2004; Brainerd et al. 2005; Azzaro et al. 2006; Warnick & Knebe 2006).

B07 demonstrate that anisotropy measurements can be strongly affected by the sample selection. It is then also likely that sample selection is critical in a measurement of the distribution of satellite orbits. Therefore, we focus on the two existing samples that B07 demonstrate, based on comparison to mock galaxy catalogues, truly select dynamically isolated systems—the original ZSFW sample and the SDSS sample constructed by B07. By combining the results from the ZSFW study with new rotation measurements of primaries drawn from B07, we increase the sample of satellites with measured orbital direction by 86, nearly doubling the ZSFW sample size (91 ZSFW satellites satisfy the selection criteria used here). The sample selection is described in §2, our observations and data reduction in §3, results, in particular our findings regarding the dynamical connections between the outer halo and inner galaxy, in §4, a brief discussion in §5, and our summary and conclusions in §6.

2 SAMPLE SELECTION

The key ingredient in any dynamical analysis of a sample of satellite galaxies is the purity of the satellite sample. Purity requires a sample of isolated primary galaxies and minimal contamination of the satellite population by interlopers along the line of sight. The value of large surveys like 2dFGRS and SDSS lies primarily in the ability to accurately identify such isolated systems, rather than in the absolute increase in size of the satellite sample. In other words, the uncertainties inherent in certain previous results, such as the Holmberg effect (e.g. Zaritsky et al. 1997b; Sales & Lambas 2004; Brainerd et al. 2005), are not principally statistical — even the early work (Zaritsky et al. 1997b) detected the asymmetry with > 99% confidence at radii > 250 kpc. B07 demonstrated that conflicting results among studies (Sales & Lambas 2004; Brainerd et al. 2005, etc.) were caused by differences in the sample selection, not small number statistics.

We use a sample of nearby isolated galaxies selected from SDSS-DR4 (Adelman-McCarthy et al., 2006) by B07 with 3600 km s⁻¹ $< v_{rec} < 38000$ km s⁻¹ (no cut on depth beyond B07 was made). The criteria B07 used to define this sample were refined using mock catalogues generated from cosmological N-body simulations. B07 conclude that many previous studies are heavily contaminated by groups, and that the isolation criteria must be stringent in order to select truly isolated systems. Their isolation criteria are tailored to (1) minimize the number of 'interlopers', or satellite-primary pairs that do not represent physical satellites of the primary galaxy, (2) minimize the number of primaries that are not isolated and so do not dominate the dynamics of their environment, and (3) maximize the sample size.

The sample from which we selected targets for follow-up was extracted from the SDSS-DR4 while the selection criteria of B07 were still being refined, and therefore there are slight differences between our sample and that of B07. The main differences are (1) our sample contains no constraint on proximity to the spectroscopic survey edge (although the

more important constraint on proximity to the photometric survey edge is included), and (2) the issue of spectroscopic incompleteness (after checking NED¹ for spectra of any potential violators not already in SDSS-DR4) is dealt with differently.

The question is whether to exclude potential primaries on the basis of projected neighbors that are sufficiently luminous to violate the isolation criteria, if they indeed lie sufficiently close in redshift to the primary. We, as is done in B07, refer to the number of such galaxies around one of our primaries as N_{viol} . ZSFW adopted a goal of $N_{\text{viol}} = 0$, although given their visual magnitude classification and lack of supporting materials at the time it is quite possible that some of their primaries do not satisfy this criteria. B07 also adopt $N_{\text{viol}} = 0$, but in an effort to minimize the number of systems rejected they use the photometric redshift information provided by SDSS to reject only systems with violators that have a photometric redshift consistent with that of the primary. Given the errors on photometric redshifts, this is still quite a conservative criteria because many of the potential interlopers will turn out to be at redshifts sufficiently distinct from that of the primary. We were initially much more liberal, not having the photometric redshifts when our sample was chosen. The critieria for our sample is $N_{\text{viol}} \leq 4$. Now that photometric redshifts are available, we revisit our sample. Of the 78 Bok-observed satellites in our sample, 17 have potential violators whose photometric redshift is consistent with that of the primary. Eleven of the 12 primaries from which these 17 satellites are drawn are found to have only one such violator and one has two such violators, and so, with one exception, our sample satisfied $N_{\text{viol}} \leq 1$. Our results are qualitatively unchanged when these 17 satellites are excluded.

Lastly, we also require that the maximum number of satellites allowed around any given primary, $N_{\rm satmax}$, is four. This criterion is set to ensure that the primary galaxy dominates the satellite system and to eliminate systems that are clearly groups rather than isolated galaxies. ZSFW do not use such a criterion, and as a result one system in their final sample (NCG 1961) has 5 associated satellites. See \S 4.1 for a description of the (minimal) effects of this system on our results.

For completeness, we correct heliocentric v_{rec} values for Galactic rotation and Virgocentric infall as described in Zaritsky et al. (1993), although these corrections are negligible over these volumes and affect only our determination of the distance to the system. Angular diameter distances and distance moduli are calculated assuming $\Omega_m = 0.3$, $\Omega_{\Lambda} = 0.7$ and $H_0 = 70 \ \mathrm{km \ s^{-1} \ Mpc^{-1}}$.

We work on a subset of the B07 sample that satisfies three additional criteria. First, we visually select a strictly disc-like (\sim S0 type or later) sample requiring the galaxies to appear to be inclined discs. This criterion is applied so that there is a well defined disc major axis and the inclination can be unambiguously measured. We then select primaries with inclinations larger than 25° (where 0° is face-on) to increase our chances of measuring the disc rotation sense. Finally, we remove any obviously disturbed systems (e.g. clear mergers or warps) because such systems, although perhaps

satisfying the broader isolation criteria, are unrepresentative of the typical isolated galaxy in our sample and likely have ambiguous disc/halo alignments. In all, these additional criteria yield a base sample of 249 primaries that we draw from during the observations (see § 3).

We will combine the results obtained from this sample to the results presented by ZSFW, which B07 confirm to have selection criteria resulting in a sample of similarly isolated primary galaxies.

3 OBSERVATIONS, DATA REDUCTION & ANALYSIS

The SDSS catalogues provide positions, magnitudes and radial velocities for the primary and associated satellite galaxies in the B07 sample. To measure whether the satellite is on a prograde or retrograde orbit we need to measure the sense of the rotation of the primary galaxy on the sky. We use the Boller & Chivens (B&C) Spectrograph on the Steward Observatory 90-inch (2.3 m) Bok Telescope (Kitt Peak, AZ) and observe 126 primary galaxies with 151 associated satellites (~ 1.2 satellites per primary) from the 249 primaries available in our base sample (see § 2). We use the 600 g/mm grating blazed at 4458 Å and centered at $\lambda \sim 5000$ Å to observe a spectral range that includes the Ca II H & K absorption lines and the H β and [O III] emission lines. This setup provides a spectral scale of 1.9 Å pixel⁻¹ and a spatial scale of 0.33'' pixel⁻¹. We use the 2.5'' wide slit and achieve a typical spectral resolution of ~ 6 Å. Exposure times range between 1200 - 1500 seconds. We obtained the data from three separate bright runs between October 2005 and April 2006. Because we simply aim to determine which side of the galaxy is rotating toward or away from us, we do not require high precision or absolute velocity calibrations.

To observe a galaxy rotation curve, one would normally align the spectrograph slit with the major axis. Given our cruder requirements, our goal of maximizing the number of observed targets, and the inefficient way in which the slit is rotated in this spectrograph, we decided to observe all of our targets with a limited set of slit angles. We chose to deviate by not more than 22.5° from the primary's major axis and therefore used one of four slit angles 45° , 90° , 135° and 180° to observe every galaxy. Because the entire B&C Spectrograph rotates with the slit, we take calibration frames at each slit angle to account for instrument flexure.

We reduce the images in the standard manner, including bias subtraction and flat fielding using standard IRAF routines². We rectify the images using a calibrated HeNeAr exposure and then subtract the background along columns. The center of the galaxy spectrum along the spatial direction is identified by the APALL task and an aperture that is between 1 and 3 pixels wide is extracted. We generally adopt the 3 pixel aperture to increase the signal-to-noise, but occasionally test whether smaller apertures result in a more statistically significant final result. The extracted spectrum serves as the template for a cross-correlation analysis of the

 $^{^2\,}$ IRAF is distributed by the National Optical Astronomy Observatories, which are operated by the Association of Universities for Research in Astronomy, Inc., under cooperative agreement with the National Science Foundation.

4 S. Herbert-Fort et al.

other rows. Row by row, we cross-correlate the spectrum and the central template using XCSAO. We accept results only for rows with significant R values (R>4) and then fit a line to the relative radial velocity as a function of row number. A significantly non-zero slope provides a measure of the sense of rotation along the slit.

For quality assurance every derived rotation curve and 2-D spectrum is visually inspected. To assist with the latter, we fit and subtract a low order continuum row-by-row. This step increases the visibility of the absorption or emission lines. If the correlation analysis appears to be strongly affected by an artifact in the data (e.g. residual cosmic ray signal, bad pixels or columns), we reject this primary from the sample (<5% of all cases). We reach a final conclusion regarding the rotation sense of the primary galaxy using both the cross-correlation analysis and our visual inspection of the spectrum. We emphasize that there is no simple relationship between slit position or detected primary rotation sense and the location and velocity of a satellite. Our interactive analysis therefore can not incorporate any bias in the determination of the satellite orbit.

We then combine the sense of primary rotation along the slit with the orientation of the slit on the sky, the position of the satellite on the sky, and Δv_{rec} to determine whether the satellite is on a projected prograde or retrograde orbit. In Figure 1, we illustrate this process with an example merging the SDSS and Bok observations. On the left we show our slit orientation overlayed on an SDSS negative image of the primary galaxy. An arrow indicates the direction toward the associated satellite. The radial velocity difference between the satellite and this primary is ~ -320 $\mathrm{km\ s}^{-1}$, i.e. the satellite is approaching us with respect to the primary. In the right panel, we show a portion of our Bok B&C sky-subtracted spectrum (longer wavelengths to the right), with a contaminating stellar spectra (having an unusual appearance due to the continuum subtraction) visible in the upper portion and the H β and [O III] emission lines of the galaxy providing the primary's rotation sense visible in the lower portion. This particular example serendipitously includes the star which helps confirm our calculation of the slit orientation on the sky. In this case, the spectrum of the lower side of the galaxy (that closest to the approaching satellite, or that toward the bottom of the CCD image) is blueshifted, indicating that the satellite is on a projected prograde $v_r \sim +320 \text{ km s}^{-1}$ orbit. Our adopted convention is to use positive (negative) velocities, v_r , to denote prograde (retrograde) orbits.

Of the 126 targeted primaries, we successfully measure the rotation sense of 63 primaries with 78 associated satellites. In Table 1 we present those primaries for which we were able to measure a rotation sense and the information about their satellite systems. This is the Bok-observed sample that we use in our analysis. For completeness, in Table 2 we present the 63 primaries for which we were unable to measure a rotation sense. The majority of the failures appear to be weak-lined sources where our signal-to-noise was insufficient. However, a significant fraction are also low-inclination ($inc < 50^{\circ}$) systems for which measuring a rotation sense is more difficult. In Figure 2 we show the distribution of primary inclinations for the 118 primaries we use in our analysis (shaded), which includes the 63 Bok-observed primaries (hatched linestyle) and the 55 ZSFW primaries. Our sam-

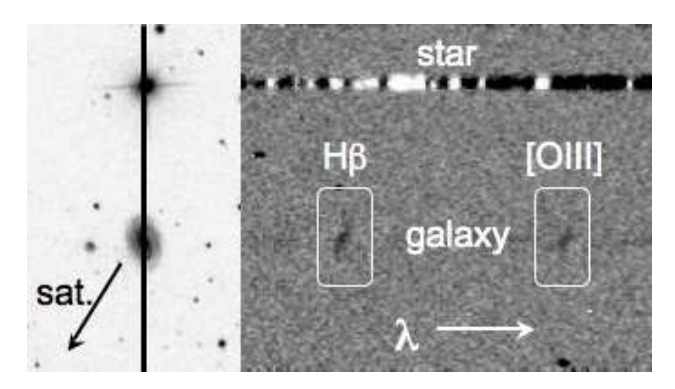


Figure 1. Combining the SDSS data and Bok observations. On the left we show our slit/primary galaxy alignment (SDSS negative image), with an arrow indicating the direction of the associated satellite. The right panel shows a cut of our Bok B&C sky-subtracted spectrum, with the contaminant stellar spectra (note the star in the slit in the SDSS image to confirm the orientation; the stellar continuum appears unusual here due to the continuum subtraction), and the H β and [O III] emission lines of the galaxy below providing the primary's sense of rotation. See the text for more details.

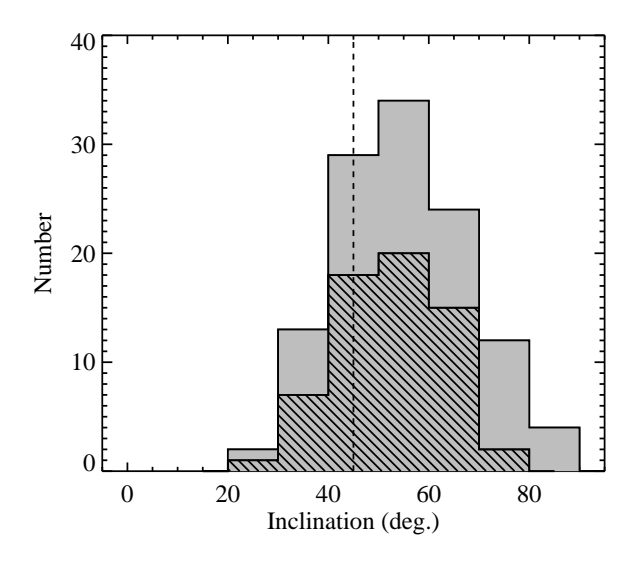


Figure 2. Distribution of inclination angles of the primary galaxies used in the analysis. The full sample is shaded and those observed specifically for this study are in hatched linestyle.

ple is therefore not in any sense random in orientation and simulations that attempt to reproduce these observations should begin with a sample that matches our distribution of primary inclinations.

4 RESULTS

4.1 Deviations from Gaussianity

In Figure 3 we show the projected rotation velocities for satellites in the Bok-observed sample (hatched linestyle) and the combined Bok + ZSFW sample (shaded). There are

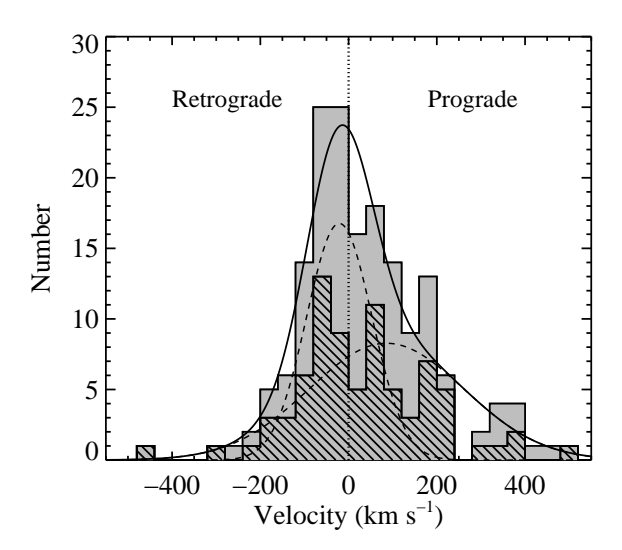


Figure 3. Radial rotation velocities in $40~\rm km~s^{-1}$ bins. The new Bok sample is shown in hatched linestyle and the overall (Bok + ZSFW) sample is shaded. Positive values depict satellites rotating in the same sense as the disc, while negative values indicate counter-rotating satellites. These data are inconsistent with a normal distribution at the > 99.9 % CL. A double-Gaussian model provides an acceptable fit to the distribution (solid linestyle, with the individual Gaussian components in dashed linestyle).

Note: these fit parameters were derived from the $unbinned\ v_r$ distribution using a maximum likelihood approach. They are not a fit to the binned distribution shown here.

three general features that are present in both the Bok and ZSFW samples: 1) a deviation from Gaussianity, 2) an asymmetric tail toward large prograde velocities, and 3) a slightly off-center peak at low retrograde velocities. We confirm the visual impression of non-Gaussianity using the Bera-Jarque test for normality (Bera & Jarque 1980), which uses the unbinned v_r distribution, at the >99.9% confidence level.

We explore the asymmetry further by testing the statistical significance of the asymmetric tails. We calculate the probability, for the combined sample, of finding P or more satellites with $v_r > X$ km s⁻¹ and N or less satellites at $v_r < -X$ km s⁻¹ using Binomial probabilities and adopting an equal chance for positive and negative velocities. Of course, this is an a posteriori test if we choose a particular value of X and hence we do the calculation for all values 0 < X < 300 km s⁻¹ (for X > 306 km s⁻¹ we have ten or fewer satellites). For values of X > 50 km s⁻¹ we find that the probability of randomly generating the observed asymmetry toward prograde orbits is < 5%, while for X > 60 km s⁻¹ the probability is always < 2%. We conclude that the asymmetry is statistically significant under the assumptions that prograde and retrograde orbits are equally likely and that each satellite is an independent measurement.

However, the assumption that each satellite is an independent dynamical tracer is questionable. Two of the systems among the largest prograde velocities are from a single primary, ZSFW's NGC 1961, which was identified by ZSFW as being notably different than the rest of the sample because of its unusually large circular velocity (551 km s $^{-1}$ width of the neutral hydrogen profile at 20% peak inten-

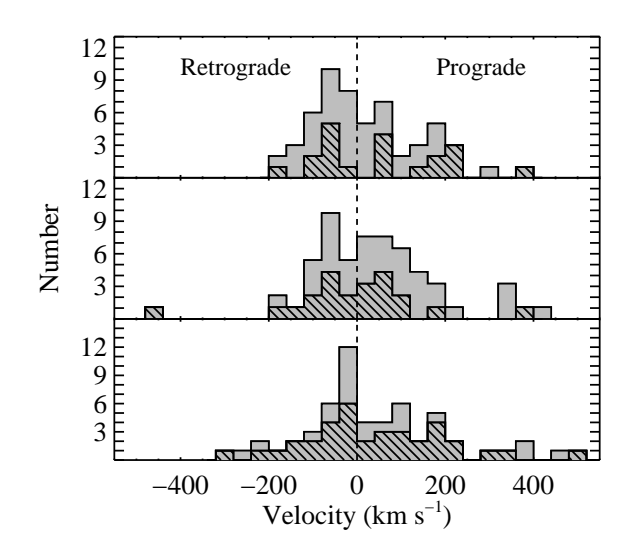


Figure 4. Rotational velocity distributions in projected radii bins (from top) [0 - 162], [162 - 368], and [368 - 750] kpc, each containing 56, 56, and 57 satellites, respectively. The overall asymmetric distribution is apparent throughout the halo.

sity) and large number of satellites (five). If we remove the NGC 1961 satellite system from the sample (it has one more satellite than the cut imposed by B07 for their sample, $N_{\rm satmax}=4$), we calculate that for $55 < X < 300 \ \rm km \ s^{-1}$ the probability of the asymmetry remains < 5%. Interlopers, which are expected at the $\sim 5-10\%$ level (Bailin et al. 2007), will not correlate with the primary's sense of rotation and therefore will not produce v_r asymmetries. We therefore conclude that the asymmetries at large v_r are statistically significant and physical.

We return now to the peak at low retrograde velocities, which is evident in both the Bok and ZSFW samples. In Figure 3 we show the result of fitting a double-Gaussian model to the unbinned v_r distribution using a maximum likelihood approach. We find that the distribution can be described as the sum of a slightly retrograde component containing $\sim 45\%$ of the sample peaked at $-21\pm22~\rm km~s^{-1}$ with standard deviation $\sigma=74\pm18~\rm km~s^{-1}$, and a broad prograde component containing $\sim 55\%$ of the sample peaked at $86\pm30~\rm km~s^{-1}$ with $\sigma=176\pm15~\rm km~s^{-1}$. These parameters agree to $\sim 1\sigma$ with the values derived from a double-Gaussian best-fit to the binned data that has a reduced $\chi^2\sim 0.6$. The maximum-likelihood fit parameter values derived from just the Bok- and ZSFW-only subsamples are consistent with those from the main sample.

In Figure 4 we plot the v_r distribution in three radial bins to illustrate that the asymmetric shape is found at all radii. The maximum-likelihood double-Gaussian fit parameters in each radial bin are roughly consistent (between $1-2\sigma$) with those from the main sample. We also look for any trends with primary inclination and disc angle (the latter being the angle between the satellite position on the sky and the nearest semi-major axis of the host primary disc) and find these slow retrograde satellites scattered throughout (see Figures 5-8).

The only suggestion of a dependence we find between the satellite velocity distribution and primary galaxy prop-

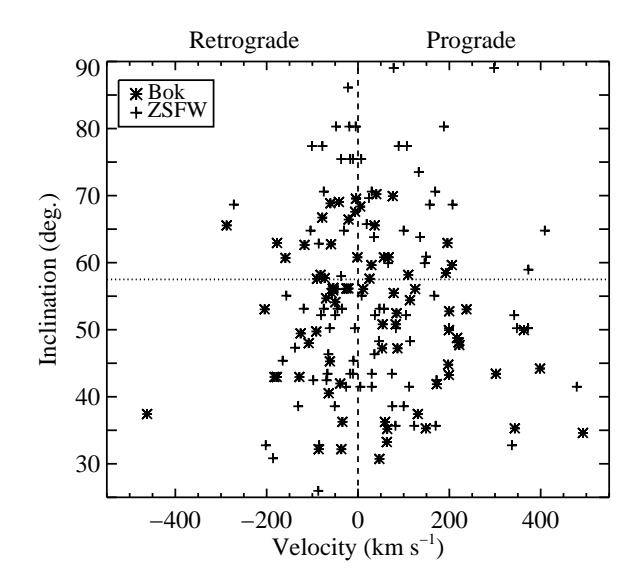


Figure 5. Rotational velocity vs. primary inclination angle. A dotted line is drawn at 57.5° (the midpoint of the inclination range considered) to guide the eye.

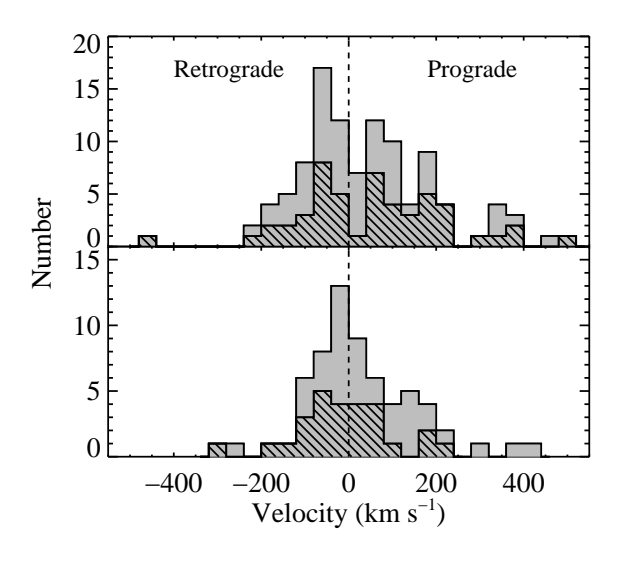


Figure 6. Rotational velocity distributions in inclination bins (from top) $[25^{\circ} - 57.5^{\circ}]$, $[57.5^{\circ} - 90^{\circ}]$. As Figure 5 suggests, the overall asymmetric distribution is apparent across the range of primary inclinations.

erty is that with primary absolute magnitude (see Figure 9), in which the asymmetry toward large prograde velocities becomes more pronounced for brighter primary galaxies (we find no dependence on satellite absolute magnitude or primary-satellite magnitude difference). Dividing the sample into 'bright' and 'faint' subsamples on either side of the median primary M_B , -20.5 mag, illustrates that it is the bright subsample that more distinctly follows the pattern of the overall two-component distribution (Figure 10). The satellite velocity distribution for the faint primary subsample (Figure 11) is closer to that of a single Gaussian, although using the statistical test for normality on the unbinned val-

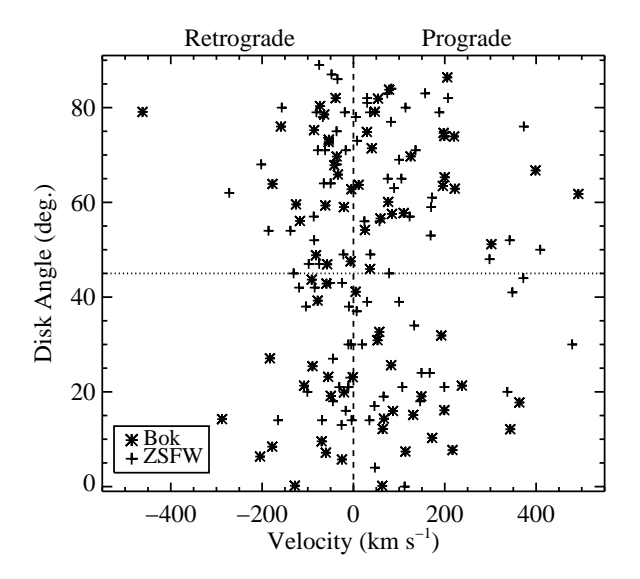


Figure 7. Rotational velocity vs. projected satellite disc angle (angle between the satellite and the nearest semi-major axis of the host primary). A dotted line is drawn at 45° to guide the eye.

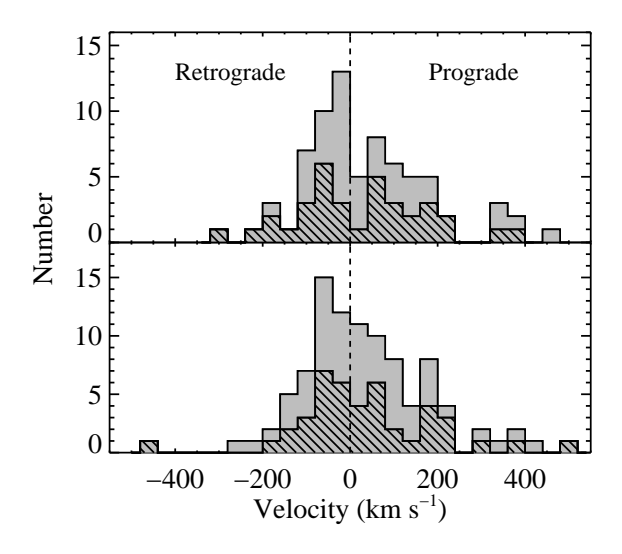


Figure 8. Rotational velocity distributions binned by satellite disc angles (from top) $[0^{\circ} - 45^{\circ}]$, $[45^{\circ} - 90^{\circ}]$. As Figure 7 suggests, the overall asymmetric distribution is apparent across the range of disc angles.

ues shows that even this distribution is inconsistent with a single Gaussian at the > 99% CL. These results may reflect a true physical difference among satellite orbits of bright and faint primary galaxies, or the ease with which one can distinctly separate the prograde component for the brighter primaries, which will be centered at larger mean velocity in the more luminous systems (see e.g. Guzik & Seljak 2002).

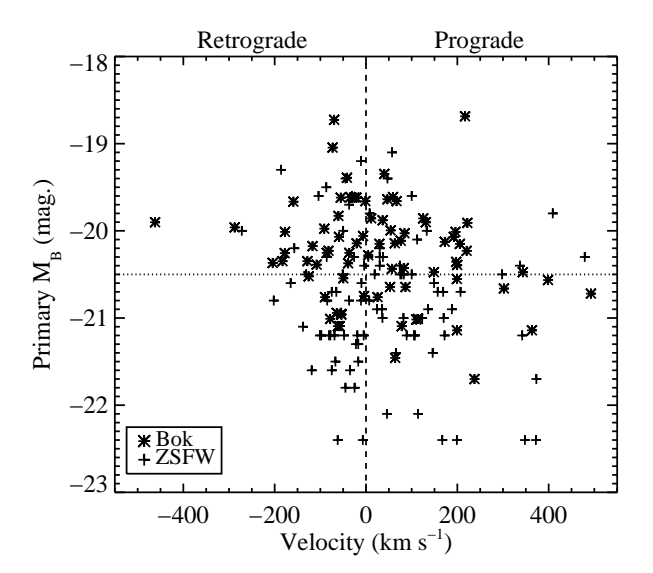


Figure 9. Rotational velocity vs. primary absolute magnitude. The median primary $M_B, -20.5$ mag., is traced by the dotted line

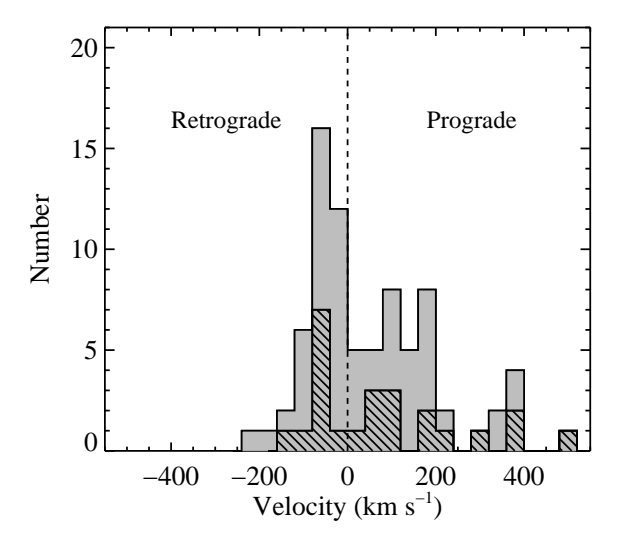


Figure 10. Rotational velocity distribution for satellites around the 'bright' primary subsample. The narrow retrograde and broad prograde components are clearly distinguished here.

4.2 The Normalised Distribution

When stacking objects it is always difficult to know if one can simply combine the sample without accounting for the differences among individual objects. In our case, we have combined satellites of primaries with different luminosities, and hence rotation speeds. One natural alternative to our straight-forward stacking is to rescale the satellite-primary velocity differences by primary rotation speed before stacking. We estimate the primary's circular velocity using the Tully-Fisher (TF) relation of Pizagno et al. (2007), $\log(V_{80}) = -0.136 \times (\mathrm{M_g} + 20.607) + 2.209$, where V_{80} is approximately the circular velocity, v_{circ} , and we have replaced $\mathrm{M_g}$ with our $\mathrm{M_B}$ values.

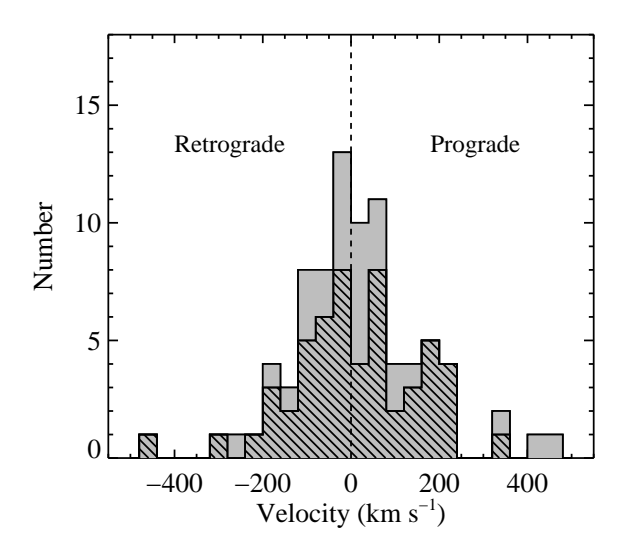


Figure 11. Rotational velocity distribution for satellites around the 'faint' primary subsample. The unbinned data here remain inconsistent with a single Gaussian at the > 99% CL, but there is little evidence for the two components.

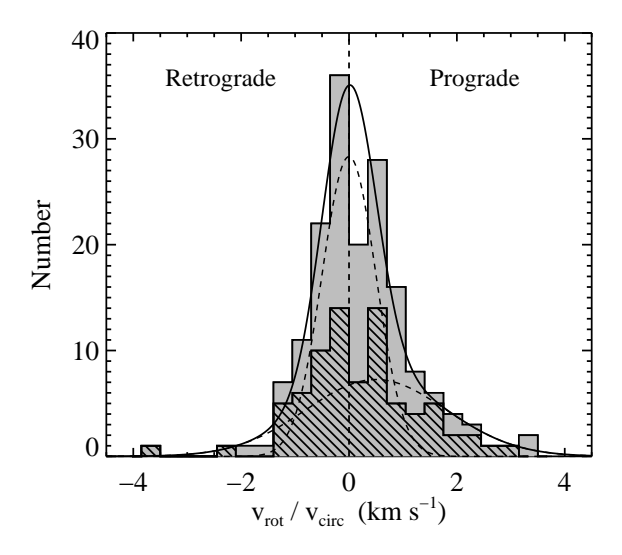


Figure 12. Projected orbital velocity distribution, normalised using the Tully-Fisher relation of Pizagno et al. (2007), in 0.35 v_{rot}/v_{circ} bins. The double-Gaussian fit was found using a maximum likelihood approach to the *unbinned* v_{rot}/v_{circ} distribution and is not a fit to the binned distribution shown here.

The normalised satellite velocity distribution, shown in Figure 12, is still asymmetric and remains inconsistent with a normal distribution at the > 99.9% CL. For completeness, we present the double-Gaussian best-fit parameters derived from the unbinned distribution using a maximum likelihood approach: we find the left-most peak centered at 0.0 ± 0.2 with standard deviation $\sigma = 0.6 \pm 0.1$, and the broad prograde peak at 0.5 ± 0.3 with standard deviation $\sigma = 1.3 \pm 0.2$. These results are consistent both qualitatively and quantitatively with the result from the straight-forward stacking analysis.

4.3 Comparison with Previous Results

There have been only two studies measuring the orbital sense of satellites (Zaritsky et al. 1997b; Azzaro et al. 2006), one of which we have incorporated here, so there is not much comparison possible. However, one aspect to expand upon is the method in which the distribution should be parametrized. ZSFW presented the fraction of satellites on prograde orbits, which was also used by Azzaro et al. (2006) and is 0.53 ± 0.04 in our sample. Our new value is lower, but roughly consistent (between 1 and 2σ) with results from the previous studies.

Warnick & Knebe (2006) conducted high-resolution N-body simulations of dark matter haloes in a standard ΛCDM cosmology and examined the velocity distribution and orientation of orbits of satellite galaxies. Their general result was an excess of prograde satellites; on average they find that 59% of satellites co-rotate with the host. However, Warnick & Knebe (2006) also find that the prograde fraction decreases to 53% when observing the data along a random line of sight, as we (nearly) do in practice (any biased distribution of primary inclinations angles should still be accounted for, of course). The decline of the prograde fraction is due to the technique observers use to determine the orbital sense of satellites and results in the possible misclassification of non-circular orbits as retrograde when in fact they are prograde (and vice versa). Thus, our measurement of a positive satellite prograde fraction (and those of any observers with a similar technique) may likely be an underestimate.

Alternatively, a useful value to compare with is the mean rotation velocity, which we find to be 37 ± 3 km s⁻¹ (> 12σ discrepant with zero). Note that this mean value must in fact be a lower limit to the coherent motion aligned with the disc because the primaries are not fully edge-on, the line-of-sight satellite velocities are not their full orbital velocities, and any interlopers are diluting the signal.

While both of these measures suggest the existence of bulk mean rotation of the outer dark halo in the same sense as the disc, they both fail to capture the nature of the deviations from the naively expected v_r distribution. In fact, had the fraction of satellites present in the narrow and prograde peaks been slightly different, it is quite possible that neither the prograde fraction or the mean velocity would provide statistically compelling evidence against a purely Gaussian, non-rotating halo. The full v_r distribution must be measured and modeled.

5 DISCUSSION

The presence of asymmetries in the v_r distribution confirms a connection between the inner, visible disc and the outer, dark halo. This connection reaches even beyond the galaxies' virial radii (indeed, Prada et al. 2006 also find that the haloes of simulated isolated galaxies may extend out to ~ 3 virial radii, and Warnick & Knebe (2006) find a bulk mean prograde rotation sense of subhaloes to five virial radii), further suggesting that large-scale structure plays a detectable role in determining both the disc orientation and the kinematics of the outer halo. Large-scale structure determines the tidal field around galaxies, and both the gas in host discs

and the orbits of the satellites may plausibly reflect torques from this large scale structure (such as from nearby clusters or filaments). The connection is potentially extremely valuable for constraining cosmological galaxy formation models because it ties together the physical processes that form the central galaxy and the infall pattern of nearby larger-scale structures. The complicated baryonic processes involved in forming the inner galaxy do not appear to erase this connection.

We briefly note here the work of Diemand et al. (2004), who identified dynamical signatures imprinted on the final velocity distribution of subhalos. They found, in simulations of cluster-sized dark matter haloes, that substructure has a flat-topped, non-Maxwellian velocity distribution. On this scale, which is not necessarily related to our systems, Diemand et al. (2004) find a *lack* of slow subhaloes, which they in part attribute to the tidal disruptions of slow substructure in the dense, young cluster environment. Analogous investigations of isolated, galaxy-sized haloes may provide insights into our findings.

The very recent work by Sales et al. (2007) examines satellite dynamics in isolated galaxy halos drawn from the Millennium Simulation, and hints at the way forward in terms of modeling the results presented here. While the cosmological volume covered by the Millennium Simulation is adequate, the semi-analytic population and evolution of the host halos does not provide an 'observer' with the orbital velocity distribution of the satellites. Nevertheless, it is important to note that Sales et al. (2007) find an asymmetric satellite radial velocity distribution with a distinct double-Gaussian shape in the outer halo regions (outside the virial radius) and a sharp peak at low negative (not retrograde) velocities. The authors attribute this component to infalling satellites, and the broader single-Gaussian shape (which dominates the inner regions) to a relaxed satellite population in equilibrium. While it is not clear if or why the sharp peak at low negative radial velocities would transform into the peak we see at slow retrograde velocities (when taking into account the primary orbital sense, which is not provided in the simulation), it is nevertheless very interesting to find a distinctly non-Gaussian distribution in the simulations.

Given the current limitations of the simulations, we are left to contemplate the empirical findings without much of a predictive framework. The question is then whether the double-Gaussian we use to model the v_r distribution is simply a convenient way to model a complex distribution or faithfully represents the presence of two physically distinct components. We speculate that the broad, prograde component is the classic halo. Its v/σ , 0.49, is similar to that of our Galaxy as traced by metal-poor globular clusters (0.44; Zinn 1985).

The origin of the slightly retrograde peak, albeit consistent with zero rotation, is more mysterious. Although dynamical friction is stronger for prograde orbits, and should thereby leave an excess of retrograde orbits, the effect is expected to be weak outside of 50 kpc (Quinn & Goodman 1986). We find that the excess of slow retrograde orbits extends well beyond this radius, and hence conclude that dynamical friction is not principally responsible. Given their low v_r , these satellites are perhaps a population on radially biased orbits and we may then be seeing the remnants of the

radial population (Figure 4 does suggest that the retrograde peak is most pronounced at the largest projected radii). If indeed the mean rotation is not retrograde, but rather consistent with no net rotation, then this component may be associated with the late infalling satellites identified in the simulations by Sales et al. (2007).

Under the assumption that the broad prograde component is a reliable indicator of the overall halo rotation, the fact that the velocity dispersion remains nearly unchanged when considering either the rotational or line-of-sight (LOS) velocity distributions indicates that the results presented here will have minimum impact on previous halo virial mass estimates from satellite studies (e.g. Zaritsky et al. 1993; Zaritsky & White 1994). In other words, the mean rotation is sufficiently smaller than the dispersion that unknowingly folding in the rotation velocity to the velocity dispersion does not give rise to significant errors. To be more quantitative, we find that the error introduced into the measured velocity dispersion by the rotation is less than the 1σ uncertainty in the velocity dispersion measurement.

Because of the ensemble stacking method used here, we do not discount the possibility that the observed bimodal v_r distribution represents two separate primary galaxy populations, rather than two perhaps distinct satellite populations. While it is not obvious why some primaries would tend to form with more slow retrograde satellites, for example, seeing whether or not single galaxies with sizable satellite populations like the Milky Way or M31 exhibit similar double-peaked satellite v_r distributions is a test of this interpretation. A first attempt at this test, using data of 19 M31 satellites from McConnachie & Irwin (2006) and the two recently discovered satellites And XII & XIV with measured radial velocities (Chapman et al. 2007; Majewski et al. 2007), is presented in Figure 13. Despite the irregular appearance of the distribution, a Bera-Jarque test for normality on the unbinned distribution does not reject the hypothesis that these data are drawn from a Gaussian distribution. Rescaled and overplotted in Figure 13 are our best-fit single- and double-Gaussian models to our ensemble sample (in dashed and solid linestyle, repectively). Neither model can be rejected with $> 2\sigma$ confidence, although the single Gaussian is the slightly better fit. The current sample is still too small to resolve this question.

Finally, we also caution that the dearth of slow prograde satellites may be an artifact of the selection of primaries that exhibit no signs of disturbance. Recall that we exclude any obviously disturbed or warped systems from our final sample. If slow prograde satellites cause more morphological damage to their primaries, then perhaps these disturbed systems preferentially host a majority of (observable) slow prograde satellites. However, the asymmetric v_r distribution is apparent throughout the halo to the largest radii, where the effects of satellites on the primary are negligible.

6 SUMMARY AND CONCLUSIONS

We use a sample of isolated disc galaxies drawn from the SDSS-DR4 (see Bailin et al. 2007, for details on selection criteria) and Zartisky et al. (1997) to examine the distribution of satellite orbits and uncover links between the dynamics and accretion history of the outer, dark halo

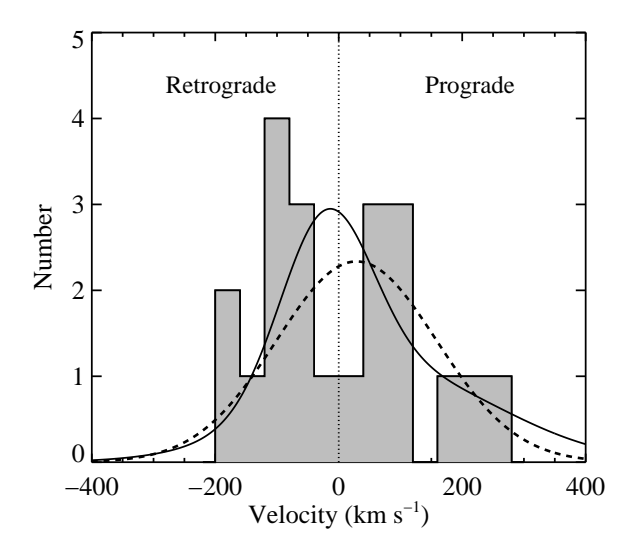


Figure 13. Projected rotational velocity distribution for satellites around M31 (see text for references). The rescaled single-and double-Gaussian fits from the ensemble sample are overplotted in dashed and solid linestyle, repsectively. The small sample size precludes any distinction between these two models.

and the inner, visible disc. We measure the rotation sense of 63 primary galaxies with 78 associated satellites using the Steward Observatory 2.3 m Bok telescope and a longslit spectrograph. Combining these data with existing radial velocity measurements, we construct the projected prograde/retrograde orbital distribution of the ensemble satellite system around an isolated, primary galaxy. When combined with the ZSFW study (91 satellites) the total sample has 169 satellites. We find a mean net bulk rotation of the satellites in the same sense as the primary, co-rotating with the host at 37 ± 3 km/s (> 12σ from zero). We caution that no corrections for interlopers have been made, but that the sample selection was tailored to minimize the effects of interlopers. We also find a prograde fraction of 0.53 ± 0.04 and caution that this is likely an underestimate of the true value (see Warnick & Knebe 2006).

The most interesting and constraining aspect of the data, however, lies rather in the shape of the projected rotational velocity distribution. We find that the data is distinctly non-Gaussian at the > 99.9\% CL, and that a double-Gaussian model with a slightly retrograde component peaked at $-21 \pm 22 \text{ km s}^{-1}$ and with standard deviation $\sigma = 74 \pm 18 \text{ km s}^{-1}$, together with a broader prograde component centered at $86 \pm 30 \text{ km s}^{-1}$ and with $\sigma = 176 \pm 15 \text{ km s}^{-1}$ provides an acceptable fit to the overall projected rotational velocity distribution. The asymmetric shape is present throughout the sample, regardless of primary inclination, projected disc angle, or radial separation, yet becomes more distinct when considering satellites of the 'bright' ($M_B < -20.5$ mag.) primaries. The nature of these results is unchanged when we scale the orbital velocities by the primary's circular velocity. We hypothesize that the two components reflect physically distinct satellite families, perhaps as suggested in a different context by Sales et al. (2007), but also discuss whether they may reflect differences among the primary galaxies.

Given the kinematic asymmetry identified here, it is evident that there remain significant underappreciated clues in the properties of satellites regarding the formation of extremely isolated galaxies.

ACKNOWLEDGMENTS

We thank the SDSS team for their impressive survey and Chris Power and Peder Norberg for helping create the mock catalogues used to define the isolated primary sample. SHF thanks Stephanie Cortes for useful discussions. SHF, DZ, and YJK were partially supported by NSF grant AST-0307482 and NASA grant LTSA NNG05GE82G. DZ gratefully acknowledges financial support during his sabbatical from the John Simon Guggenheim foundation, KITP through its support form the National Science Foundation grant PHY99-07949, and the NYU Physics Department and Center for Cosmology and Particle Physics. JB thanks the Australian Research Council for financial support, and JET gratefully acknowledges support from NSERC Canada.

Funding for the Sloan Digital Sky Survey (SDSS) has been provided by the Alfred P. Sloan Foundation, the Participating Institutions, the National Aeronautics and Space Administration, the National Science Foundation, the U.S. Department of Energy, the Japanese Monbukagakusho, and the Max Planck Society. The SDSS Web site is http://www.sdss.org/. The SDSS is managed by the Astrophysical Research Consortium (ARC) for the Participating Institutions. The Participating Institutions are The University of Chicago, Fermilab, the Institute for Advanced Study, the Japan Participation Group, The Johns Hopkins University, the Korean Scientist Group, Los Alamos National Laboratory, the Max-Planck-Institute for Astronomy (MPIA), the Max-Planck-Institute for Astrophysics (MPA), New Mexico State University, University of Pittsburgh, University of Portsmouth, Princeton University, the United States Naval Observatory, and the University of Washington.

REFERENCES

Aubert D., Pichon C., Colombi S., 2004, MNRAS, 352, 376 Adelman-McCarthy J. K. et al., 2006, ApJS,162, 38

Azzaro M., Zentner A. R., Prada F., Klypin A. A., 2006, ApJ, 645, 228

Bailin J., Power C., Norberg P., Zaritsky D., Gibson B. K., 2007, MNRAS, submitted

Bera A. K., Jarque C. M., 1980, Economics Letters, 6, 255 Brainerd T. G., 2005, ApJ, 628, 101

Blanton M. R. et al., 2003, AJ, 125, 2348

Chapman S. C. et al., 2007, ApJ, 662, 79

Diemand J., Moore B., Stadel J., 2004, MNRAS, 352, 535

Governato F., Willman B., Mayer L., Brooks A., Stinson G., Valenzuela O., Wadsley J., Quinn T., 2007, MNRAS, 374, 1479

Guzik J., Seljak U., 2002, MNRAS, 335, 311

Holmberg E., 1969, Ark. Astron., 5, 305

Knebe A., Gill S. P. D., Gibson B. K., Lewis G. F., Ibata R. A., Dopita M. A., 2004, ApJ, 603, 7

Libeskind N. I., Cole S., Frenk C. S., Okamoto T., Jenkins A., 2007, MNRAS, 374, 16

Majewski S. R. et al., 2007, astro.ph, 2635

Maller A. H., Bullock J. S., 2004, MNRAS, 355, 694

McConnachie A. W., Irwin M. J., 2006, MNRAS, 365, 902 Navarro J. F., Abadi M. G., Steinmetz M., 2004, ApJ, 613,

Okamoto T., Eke V. R., Frenk C. S., Jenkins A., 2005, MNRAS, 363, 1299

Pizagno J. et al., 2007, AJ, 134, 945

Prada F. et al., 2003, ApJ, 598, 260

Prada F., Klypin A. A., Simonneau E., Betancort-Rijo J., Patiri S., Gottlöber S., Sanchez-Conde M. A., 2006, ApJ, 645, 1001

Quinn P. J., Goodman J., 1986, ApJ, 309, 472

Sales L., Lambas D. G., 2004, MNRAS, 348, 1236

Sales L., Lambas D. G., 2005, MNRAS, 356, 1045

Sales L.V., Navarro J.F., Lambas D.G., White S.D.M., Croton D.J., 2007, MNRAS, in press

Sharma S., Steinmetz M., 2005, ApJ, 628, 21

Springel V. et al., 2005, Nature, 435, 629

van den Bosch F. C., Yang X., Mo H. J., Norberg P., 2005, MNRAS, 356, 1233

Warnick K., Knebe A., 2006, MNRAS, 369, 1253

White S. D. M., Zaritsky D., 1992, ApJ, 394, 1

Zaritsky D., Smith R., Frenk C., White S. D. M., 1993, ApJ, 405, 464

Zaritsky D., Smith R., Frenk C., White S. D. M., 1997, ApJ, 478, 39

Zaritsky D., Smith R., Frenk C., White S. D. M., 1997, ApJ, 478, 53

Zaritsky D., White S. D. M., 1994, ApJ, 435, 599

Zentner A. R., Kravstov A. V., Gnedin O. Y., Klypin A. A., 2005, ApJ, 629, 219

Zinn R., 1985, ApJ, 293, 424

This paper has been typeset from a $\text{TeX}/\text{ }\text{E}^{\text{TeX}}$ file prepared by the author.

Table 1. Bok-Observed Primary/Satellite Sample. RA & Dec listed in degrees; absolute magnitudes are on the Vega system and determined using sdss2bessel from KCORRECT (Blanton et al. 2003) v4_1_4 with SDSS redshifts and dereddened apparent magnitudes; inc $_{pri}$ are the inclinations of the primaries in degrees; r_p are the projected radii of the satellites from their host primary in kpc; θ are the projected disc angles of the satellites with respect to their host primary's nearest semi-major axis, in degrees; and v_r are the final projected rotational velocities determined for the satellites, in km s⁻¹ (positive values indicate projected prograde rotation).

RA_{pri}	Dec_{pri}	RA_{sat}	Dec_{sat}	$M_{B(pri)}$	$M_{B(sat)}$	inc_{pri}	r_p	θ	v_r
2.805	14.282	2.833	14.339	-21.0	-18.5	58	343	58	110
16.600	-0.145	16.599	-0.170	-20.3	-17.4	43	84	8	-178
18.703	-0.496	18.681	-0.549	-20.4	-17.3	44	138	75	198
23.230	14.969	23.159	14.938	-20.6	-18.5	44	367	67	399
23.281	14.761	23.100	14.727	-20.2	-17.7	48	700	74	220
27.783	-9.792	27.753	-9.761	-21.1	-17.9	45	131	59	-62
116.014	33.077	116.202	33.039	-20.7	-18.6	43	630	51	302
116.110	29.269	116.174	29.316	-19.9	-17.2	56	206	64	11
116.110	29.269	116.312	29.250	-19.9	-17.7	56	499	70	125
117.801	22.423	117.773	22.367	-20.2	-17.7	58	199	49	-82
119.194	31.929	119.223	31.925	-20.1	-18.1	63	96	43	-59
120.764	27.744	120.761	27.584	-20.1	-17.6	59	534	32	192
121.249	34.016	121.371	33.984	-20.4	-18.1	53	458	6	-204
123.003	39.013	123.060	39.049	-20.0	-17.7	51	167	82	54
123.802	41.215	123.811	41.098	-21.1	-18.9	50	502	74	199
123.802	41.215	123.766	41.194	-21.1	-18.2	50	147	18	363
125.159	36.885	125.330	36.885	-19.0	-16.7	58	297	80	-73
127.217	42.522	127.252	42.520	-20.1	-18.0	41	101	10	172
131.207	43.450	131.215	43.466	-20.8	-17.8	58	63	25	-90
131.207	43.450	131.415	43.429	-20.8	-18.1	58	578	54	25
131.771	41.715	131.770	41.702	-20.5	-18.0	54	61	19	-50
132.014	37.663	132.251	37.574	-20.4	-18.0	42	710	82	-39
136.903	3.393	137.101	3.368	-19.6	-16.7	56	186	6	-25
136.903	3.393	137.213	3.448	-19.6	-17.7	56	292	23	-55
136.903	3.393	136.764	3.818	-19.6	-15.9	56	415	59	-21
137.973	37.404	137.889	37.366	-21.7	-18.9	53	530	21	237
144.477	6.654	144.462	6.622	-21.0	-18.4	56	172	73	-54
144.516	42.974	144.572	42.973	-20.4	-18.0	61	135	33	57
144.747	6.955	144.503	6.924	-19.7	-16.4	61	297	76	-159
144.894	3.158	144.999	2.996	-20.1	-18.0	68	633	48	-6
144.908	59.791	144.546	59.746	-20.4	-18.2	48	633	21	-108
147.734	62.186	148.175	62.281	-19.4	-16.3	69	404	68	-42
148.984	53.694	149.192	53.686	-20.2	-17.5	63	380	56	-117
151.007	38.677	150.898	38.621	-20.1	-17.5	70	343	60	76
153.586	49.511	153.640	49.389	-21.0	-18.2	67	536	39	-78
154.085	4.822	153.949	4.750	-21.0	-17.6	56	501	73	-54
154.245	49.627	154.016	49.818	-20.6	-17.6	47	713	16	86
154.245	49.627	154.197	49.630	-20.6	-18.0	47	91	31	53
154.271	54.821	154.634	54.812	-20.4	-17.1	53	572	65	200
154.971	55.436	154.689	55.494	-19.6	-16.8	36	397	57	59
154.971	55.436	155.245	55.349	-19.6	-16.9	36	417	66	-34
156.430	39.646	156.397	39.674	-20.1	-18.2	33	64	0	63
157.959	54.355	157.951	54.403	-19.8	-17.8	69	162	7	-60
158.333	58.076	158.074	58.230	-20.0	-18.2	52	663	58	84
158.563	52.871	158.550	52.926	-20.0	-16.9	67	95	20	-20
160.065	65.492	160.343	65.395	-20.1 -19.9	-10.9	66	367	46	36
165.816	54.111	165.883	54.119	-19.9	-17.3	55	194	47	-58
165.816	54.111	165.759	54.074	-21.1	-18.4	55	242	84	-38 78
100.010	04.111	100.108	04.014	-41.1	-10.4	99	242	04	10

 ${\bf Table} \,\, {\bf 1} - {\it continued}$

RA_{pri}	Dec_{pri}	RA_{sat}	Dec_{sat}	$\mathcal{M}_{B(pri)}$	$\mathcal{M}_{B(sat)}$	inc_{pri}	r_p	θ	v_r
166.496	58.946	166.640	58.922	-20.4	-17.7	51	264	26	83
173.701	46.990	173.739	46.889	-20.0	-17.0	63	248	63	196
173.701	46.990	173.781	46.770	-20.0	-17.6	63	535	64	-177
173.853	57.650	173.849	57.650	-19.9	-17.0	37	5	15	131
173.853	57.650	173.792	57.579	-19.9	-17.5	37	162	79	-462
174.028	62.249	173.932	62.258	-20.1	-17.6	60	107	86	205
174.028	62.249	173.433	62.361	-20.1	-17.0	60	702	75	29
181.347	64.508	181.220	64.605	-21.5	-18.9	35	618	12	64
191.340	61.694	191.596	61.781	-20.7	-18.7	34	606	62	493
192.416	49.447	192.273	49.554	-20.6	-18.0	43	390	16	199
193.704	44.156	193.537	44.026	-20.7	-18.9	70	672	63	-4
198.250	43.204	198.285	43.217	-20.9	-18.8	40	121	79	-64
203.203	41.872	203.148	41.788	-20.3	-16.7	31	182	75	-86
203.203	41.872	203.341	42.146	-20.3	-17.5	31	573	70	-37
204.542	60.273	204.221	60.329	-20.3	-17.0	43	406	0	-128
204.542	60.273	204.841	60.293	-20.3	-17.6	43	361	27	-183
207.873	43.806	207.891	43.820	-19.9	-16.7	47	44	63	222
220.880	49.393	221.081	49.412	-19.6	-17.4	30	287	79	47
221.826	58.226	221.557	58.004	-18.7	-17.0	55	707	10	-70
222.111	34.998	222.108	35.159	-20.3	-16.8	69	341	41	5
222.912	40.599	222.731	40.524	-19.7	-15.2	61	187	23	-1
222.912	40.599	222.507	40.362	-19.7	-15.1	61	464	14	67
226.179	61.719	226.284	61.703	-18.7	-16.4	49	107	8	217
229.855	45.880	229.831	45.790	-19.3	-17.2	71	115	71	40
238.795	52.169	238.716	52.134	-20.0	-17.9	50	160	44	-91
240.751	27.010	240.649	27.212	-20.5	-17.1	35	517	19	149
240.751	27.010	240.684	27.201	-20.5	-16.5	35	466	12	343
241.370	42.627	241.180	42.712	-20.5	-17.5	49	459	60	-126
242.683	41.149	242.797	40.944	-20.0	-16.4	66	504	14	-288
355.895	0.568	355.903	0.635	-21.0	-18.7	54	376	7	114

Table 2. Bok-Observed Primaries with No Detected Rotational Sense. Same units as Table 1. Apparent magnitudes are AB SDSS Petrosian rband.

RA_{pri}	Dec_{pri}	$\mathbf{m}_{r(pri)}$	$\mathcal{M}_{B(pri)}$	inc_{pri}
27.938	-9.240	15.3	-20.7	41
113.723	39.764	15.1	-20.8	35
123.097	28.407	15.2	-20.5	28
127.257	47.801	14.4	-20.3	32
128.955	51.583	15.1	-19.5	66
134.424	43.127	13.9	-20.2	55
141.913	7.080	14.9	-20.8	56
146.196	51.689	14.3	-20.0	29
148.870	38.641	14.8	-20.7	38
148.996	6.566	15.1	-20.6	52
152.939	11.346	15.0	-20.4	38
156.349	64.999	14.8	-19.0	51
157.337	7.768	15.3	-19.0	44
157.583	8.061	14.6	-20.4	43
158.009	13.774	15.4	-21.3	63
161.873	7.251	13.7	-19.9	42
162.751	12.287	14.3	-20.2	41
164.687	59.511	13.5	-19.8	38
165.657	59.125	13.7	-20.4	67
169.969	54.463	14.3	-20.5	29
171.812	10.322	14.4	-20.6	54
173.097	54.983	14.8	-20.1	51
173.950	63.492	14.4	-19.6	54
176.858	54.407	15.3	-20.7	54
183.797	54.634	15.2	-21.3	33
184.344	53.557	14.7	-20.7	50
184.649	42.014	14.7	-20.4	57
188.135	48.472	14.6	-20.9	53
189.000	54.221	13.1	-19.4	40
189.306	49.448	13.7	-20.2	47
189.661	1.473	14.6	-20.3	66
190.146	2.468	14.4	-20.2	56
193.903	60.183	15.2	-20.8	65
194.925	43.753	14.6	-20.8	52
197.675	42.285	14.6	-19.9	48
200.872	49.013	15.2	-18.6	43
201.021	58.287	15.2	-19.7	48
204.874	46.564	14.0	-20.3	35
210.105	65.218	15.1	-20.9	50
210.689	38.066	14.9	-20.8	54
211.579	36.834	15.3	-19.8	69
222.210	57.771	14.5	-20.1	33
222.327	52.553	15.1	-20.7	46
223.321	52.044	14.4	-20.1	42
224.259	35.551	14.8	-21.1	45
226.154	48.739	14.9	-19.4	34
227.527	56.373	14.7	-20.4	52
229.589	58.112	14.6	-19.3	64
231.464	38.771	15.0	-20.2	40
232.739	36.807	14.8	-20.2	67
232.828	36.080	15.1	-19.2	32
232.952	51.768	14.5	-18.6	43
235.291	-1.706	14.0	-20.4	45

14 S. Herbert-Fort et al.

 ${\bf Table} \,\, {\bf 2} - {\it continued}$

RA_{pri}	Dec_{pri}	$\mathbf{m}_{r(pri)}$	$M_{B(pri)}$	inc_{pri}
241.073	42.028	15.0	-19.6	51
241.823	41.404	14.5	-19.8	36
241.907	45.065	14.5	-20.0	57
253.593	41.335	13.7	-20.2	33
258.118	30.910	14.5	-20.9	39
323.174	-0.128	14.4	-20.9	56
332.970	0.109	14.0	-20.2	46
335.206	-9.488	15.4	-20.9	39
349.606	14.939	15.3	-19.7	52
357.035	-10.774	15.5	-20.4	51